ADVANCED SUSTAINABLE SYSTEMS

Supporting Information

for *Adv. Sustainable Syst.,* DOI: 10.1002/adsu.202100120

High Shunt Resistance SnO_2-PbO Electron Transport Layer for Perovskite Solar Cells Used in Low Lighting Applications

Zhuoneng Bi, Shaohong Zhang, Marimuthu Thandapani, Yanqing Zhu, Yupeng Zheng, Nguyen Quang Liem, Xiudi Xiao, Gang Xu, Antonio Guerrero, and Xueqing Xu**

Supporting information

High Shunt Resistance SnO_2-PbO Electron Transport Layer for Perovskite Solar Cells used in Low Lighting Applications

Zhuoneng Bi,[1,2] Shaohong Zhang,[1,2] Marimuthu Thandapani,[1] Yanqing Zhu,[1] Yupeng Zheng,[1,2] Nguyen Quang Liem,[4] Xiudi Xiao,[1,2] Gang Xu,[1,2] Antonio Guerrero,[3*] Xueqing Xu[1,2*]

[1] Key Laboratory of Renewable Energy, Guangdong Key Laboratory of New and Renewable Energy Research and Development, Guangzhou Institute of Energy Conversion, Chinese Academy of Sciences, Guangzhou 510640, China

[2] Center of Materials Science and Optoelectronics Engineering, University of Chinese Academy of Sciences, Beijing 100049, China

[3] Institute of Advanced Materials (INAM), Universitat Jaume I, 12006 Castelló, Spain

[4] Institute of Materials Science, VAST, Hanoi, Vietnam

[*] Corresponding author

email: aguerrer@uji.es, xuxq@ms.giec.ac.cn

Preparation and characterization of SnO_2 films doped with PbO

Pb-doped SnO_2 nanoparticles were preapared from aqueous SnO_2 colloidal dispersion (15 wt%) was mixed with $Pb(CH_3COO)_2 \cdot 3H_2O$ solution. Initially, the solutions became opaque (Figure S1). After stirring the solutions in the atmosphere for 12 h, the solution became transparent again.

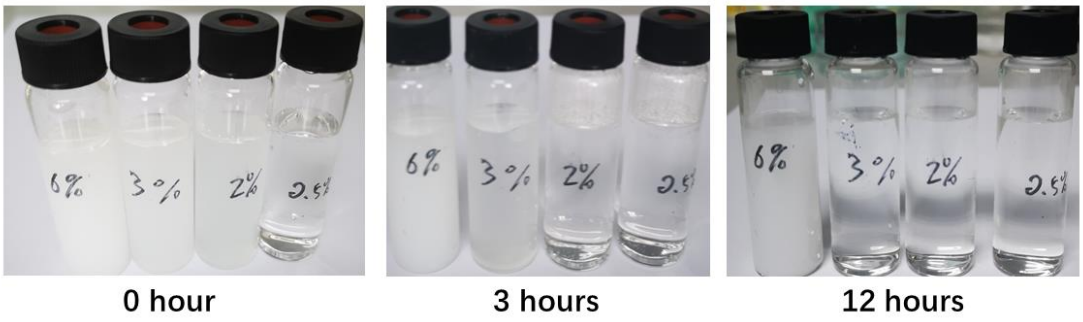

Fig. S1. photograph of process of Pb doping in SnO_2

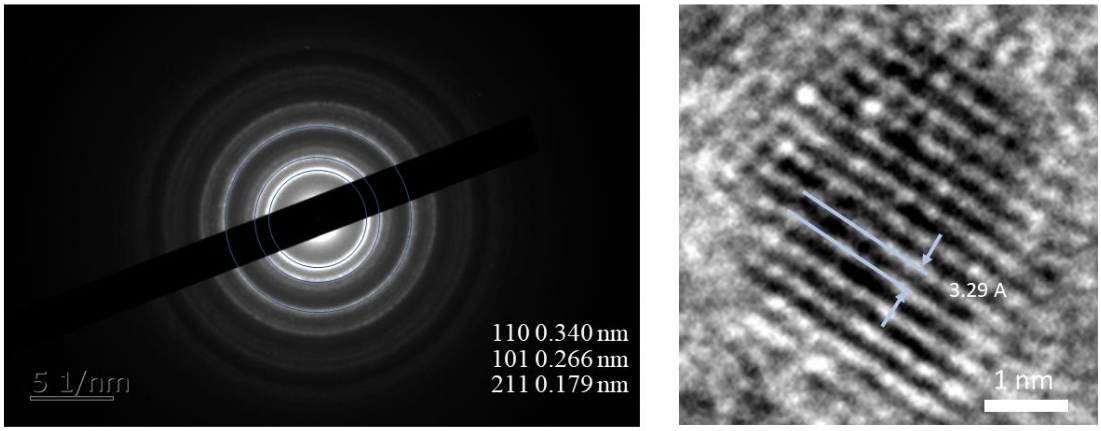

Fig. S2. TEM image of the 3% Pb doped SnO_2 nanocrystal.

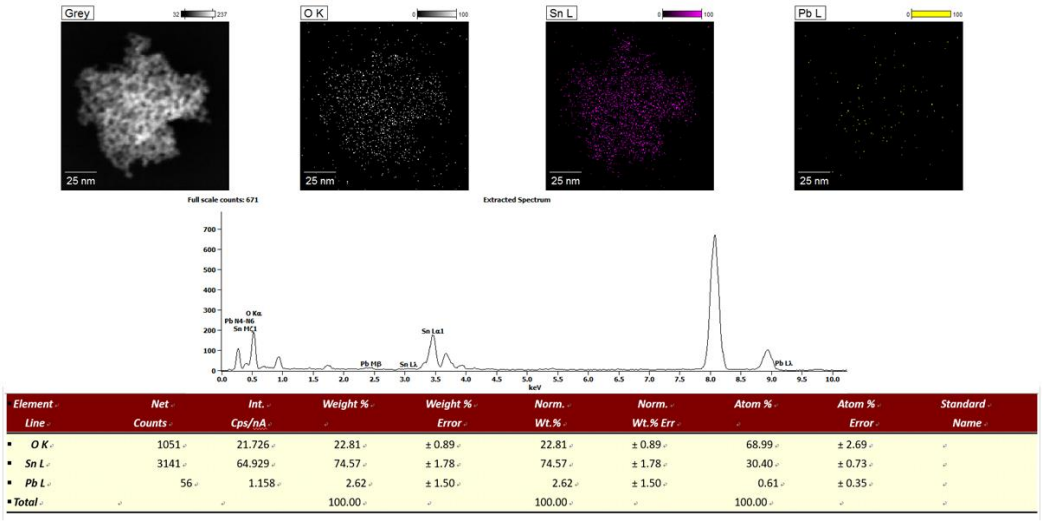

Element Line	Net Counts	Int. Cps/nA	Weight %	Weight % Error	Norm. Wt.%	Norm. Wt.% Err	Atom %	Atom % Error	Standard Name
O K	1051	21.726	22.81	± 0.89	22.81	± 0.89	68.99	± 2.69	
Sn L	3141	64.929	74.57	± 1.78	74.57	± 1.78	30.40	± 0.73	
Pb L	56	1.158	2.62	± 1.50	2.62	± 1.50	0.61	± 0.35	
Total			100.00		100.00		100.00		

Fig. S3. Elemental mapping of O, Sn, and Pb for TEM images.

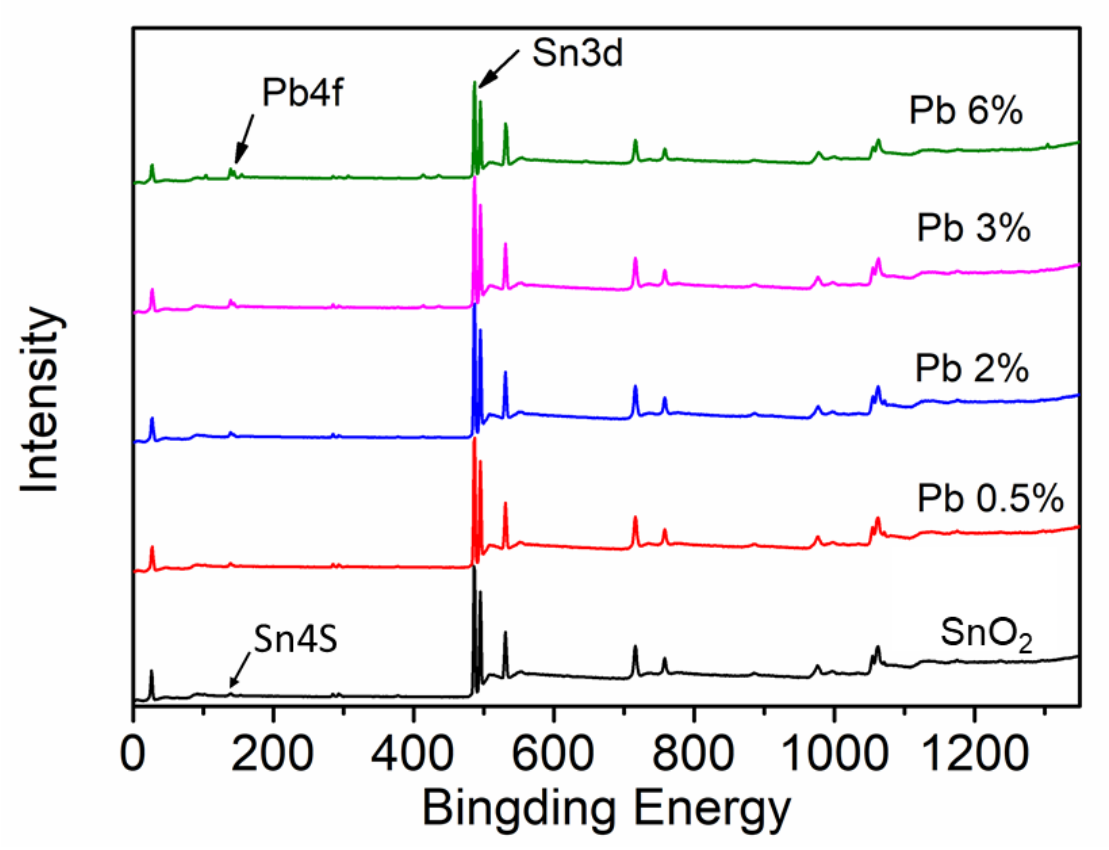

Fig. S4. XPS of SnO_2 and Pb doped SnO_2 films deposited on glass.

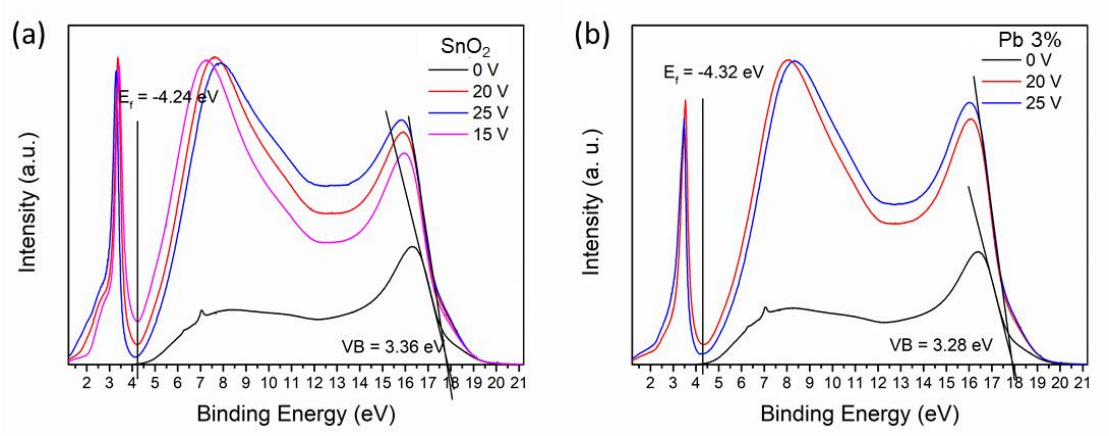

Fig. S5. UPS spectra of pure SnO_2 and 3% Pb doped SnO_2

Table S1. Atomic ratio obtained from XPS.

	O Atomic%	**Sn Atomic%**	**Pb Atomic%**	**Pb : Sn**
SnO_2	60.23	39.77	0	0
Pb 0.5%	56.57	43.33	0.11	0.254%
Pb 2%	59.10	40.56	0.36	0.887%
Pb 3%	59.10	40.15	0.75	1.868%
Pb 6%	58.23	39.44	2.32	5.882%

Structural and Optical properties of $MAPbI_3$ films from blade coating method

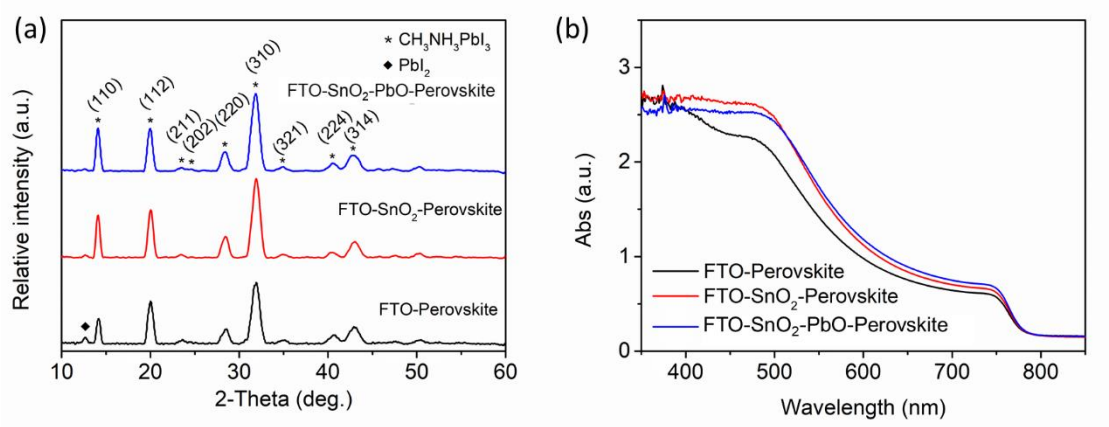

Fig. S6. a) XRD diffraction patterns of the perovskite films deposited on different substrate by doctor blade and b) Absorption spectra of perovskite films deposited on different substrate by doctor blade method in atmospheric air conditions (R.H. 30%~40%).

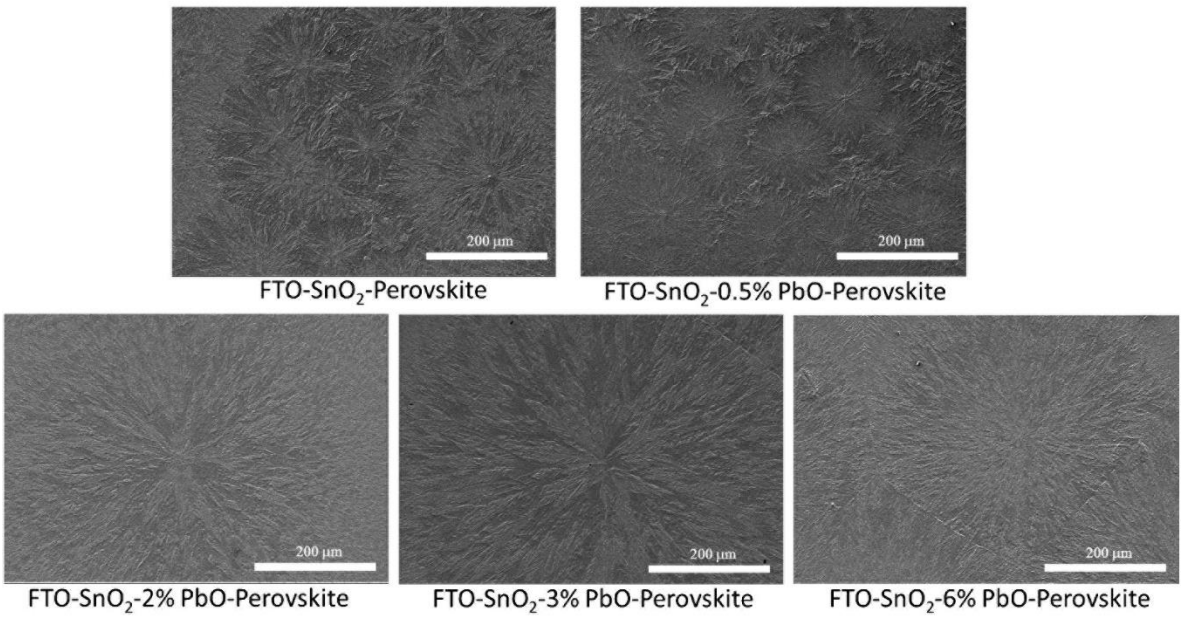

Fig. S7. Top-view SEM images of $MAPbI_3$ films at different substrate.

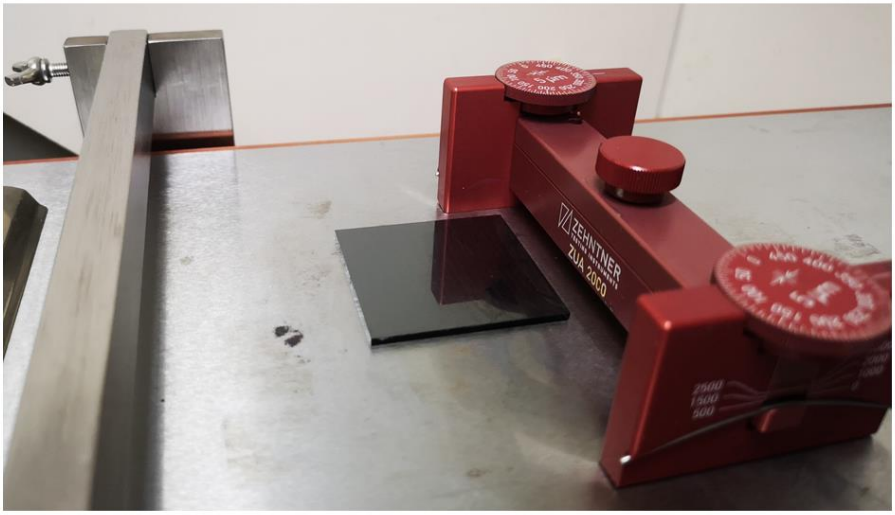

Fig. S8. Photograph of $MAPbI_3$ film with 25 cm^2.

Device performance analysis

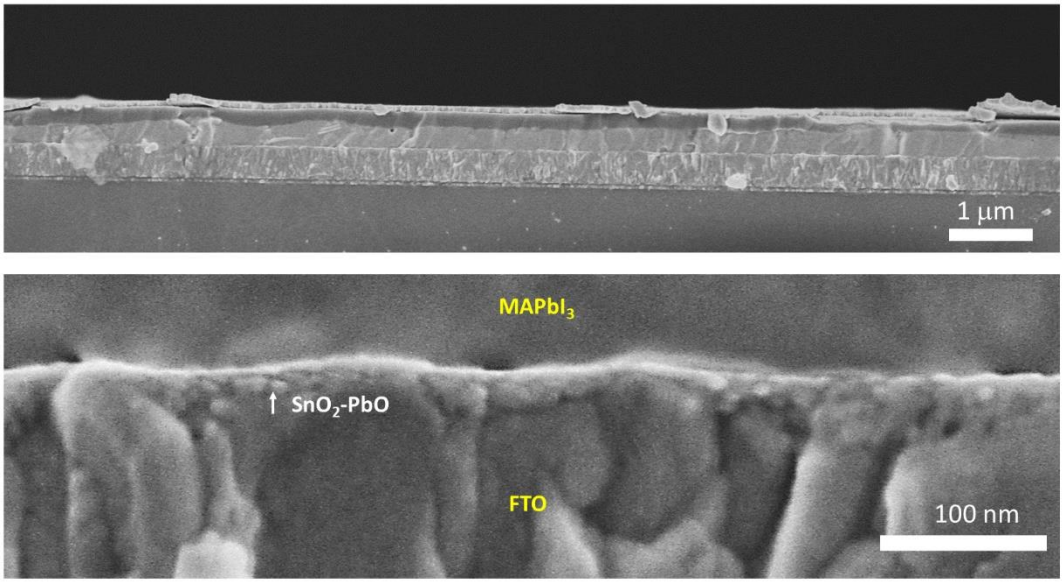

Fig. S9. Cross-Section SEM images of complete device at different magnifications.

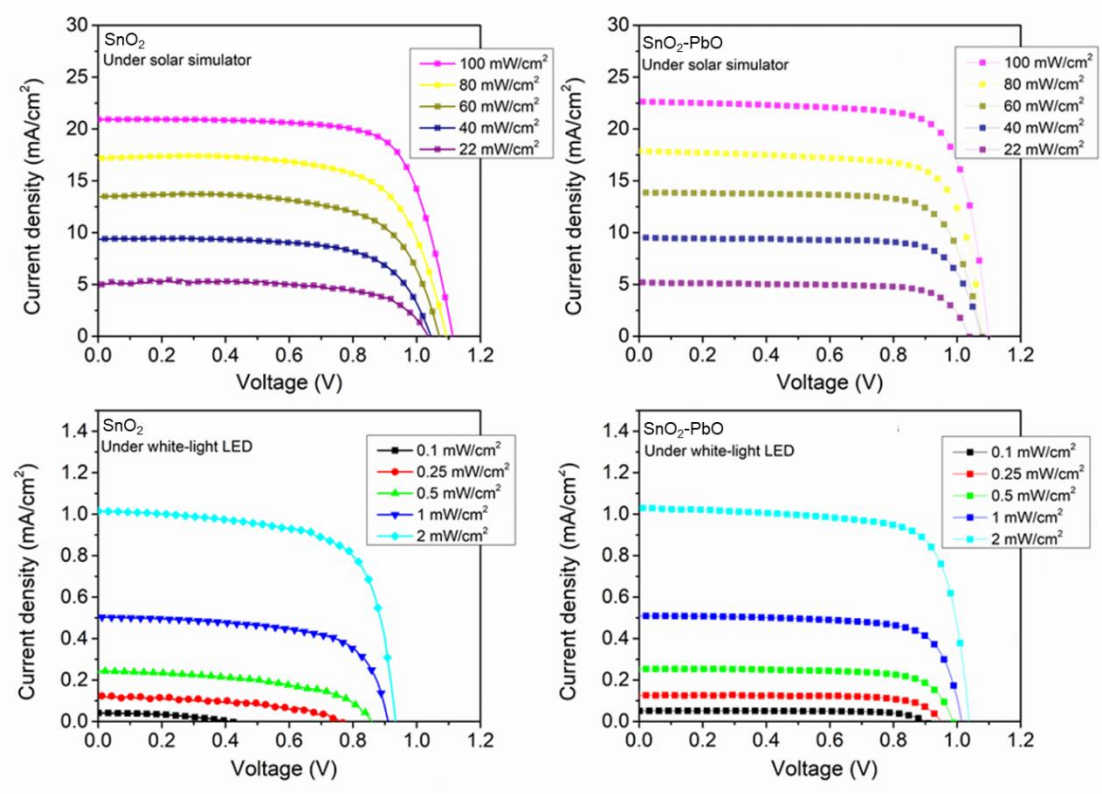

Fig. S10. *J-V* curves under different light sources and light intensity.

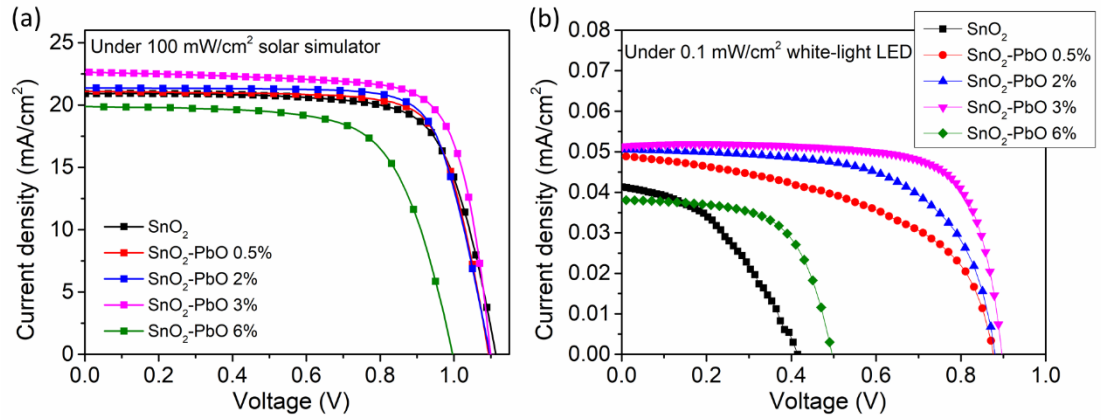

Fig. S11. *J-V* curves of bilayer Pb-doped SnO_2/SnO_2 ETLs-based devices for different Pb doping a) under 100 mW/cm2 solar simulator, b) under 0.1 mW/cm2 white-light LED.

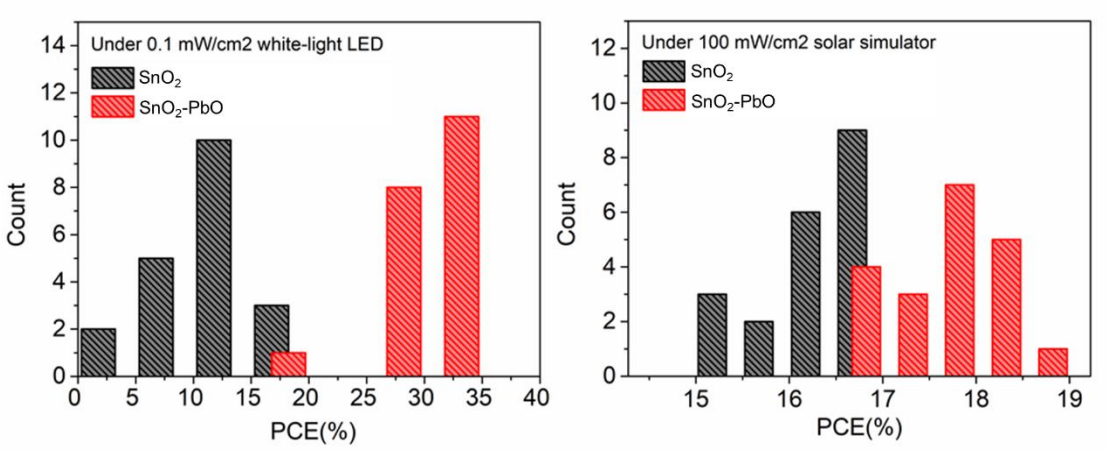

Fig. S12. PCE histogram of 20 devices.

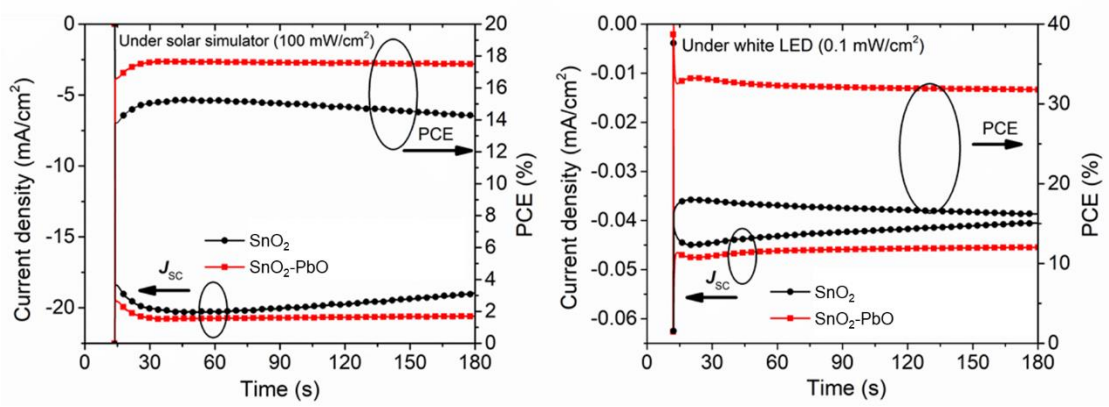

Fig. S13. Steady photocurrent and PCE measured at the maximum Power point curves.

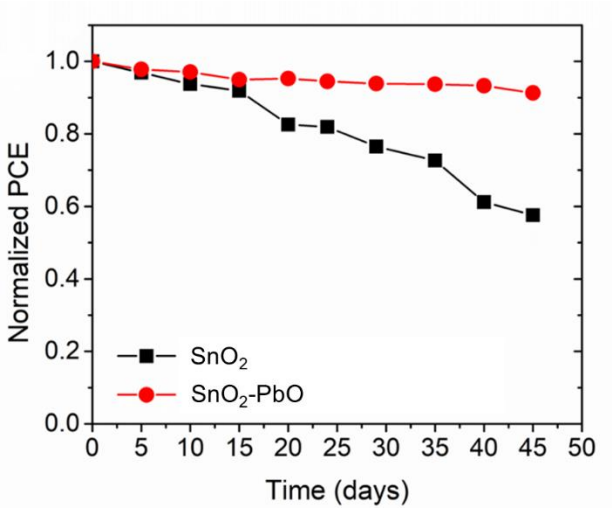

Fig. S14. Environmental stability test of PSCs devices based on SnO_2 and SnO_2-PbO under dark continuous at room temperature and under around 15% humidity.

Fig. S15. Photo shown the high shunt resistance perovskite solar cells provide power to the green LED under low lighting condition (~387 lux).

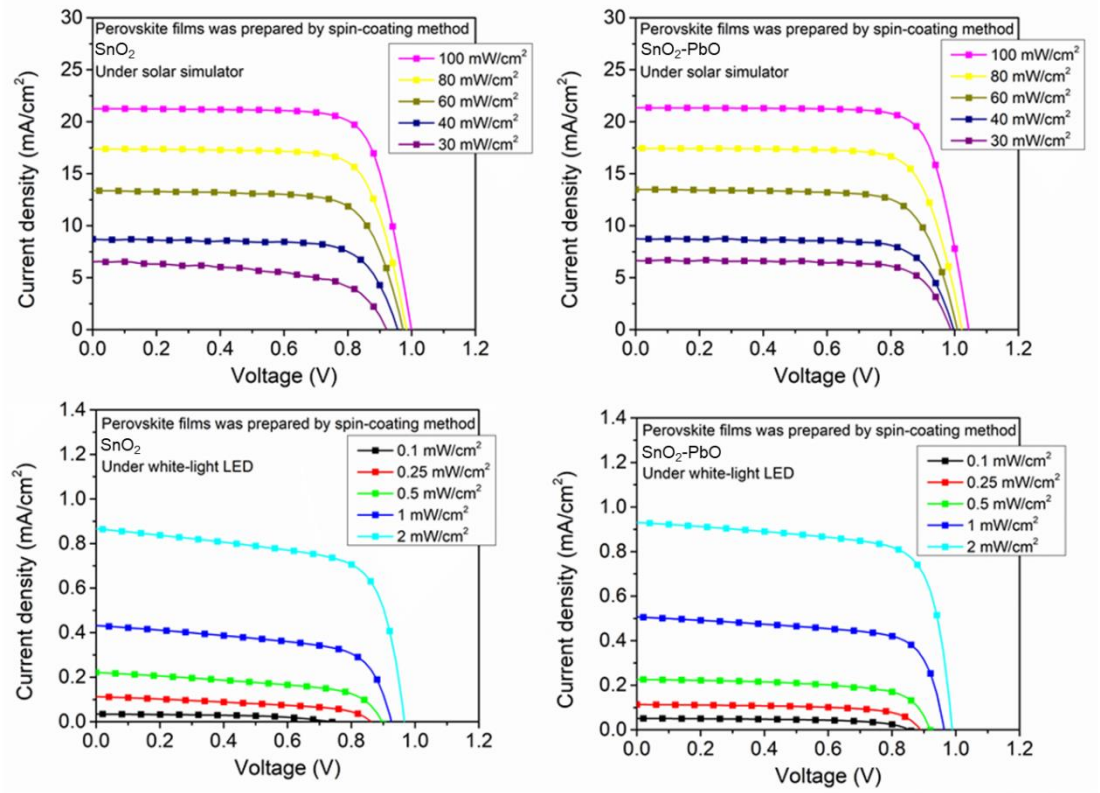

Fig. S16. *J-V* curves of PSCs that perovskite films were prepared by spin-coating method.

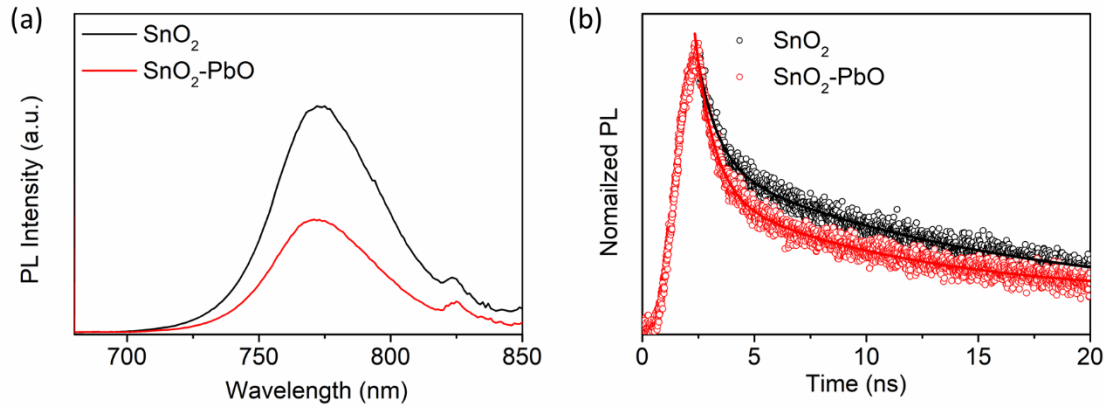

Fig. S17. a) Steady-state PL and b) time-resolved PL (TRPL) spectra of perovskite films deposited on SnO_2 and SnO2-PbO.

Device Modeling

Device parameters acquisition: The single diode model (Figure 6a) can be adopted according to the *J-V* characteristic of an ideal single heterojunction solar cell as follows:[1]

$$J = J_{ph} - J_0[\exp(q(V + JR_s)/AK_BT) - 1] - (V + JR_s)/R_{sh} \quad (1)$$

where J and V are terminal current density and voltage respectively, J_0 is the reverse saturated current density, A is the junction ideality factor. K_B is the Boltzmann constant, T is the absolute temperature, and q is the elementary charge, R_s and R_{sh} are series and shunt resistance, respectively. Since R_{sh} is very high in an ideal heterojunction solar cell, and at higher applied bias, formula (1) can be simplified as follows:

$$J = J_{sc} - J_0[\exp(q(V + JR_s)/AK_BT)] \quad (2)$$

Hence following equations can be derived from formula (2):

$$-\mathrm{d}V/\mathrm{d}J = AK_B\mathrm{T}(J_{SC} - J)^{-1}q^{-1} + R_s \quad (3)$$

$$\mathrm{In}(J_{SC} - J) = (\mathrm{V} + R_sJ)qA^{-1}K_B^{-1}T^{-1} + \mathrm{In}(J_0) \quad (4)$$

$$V_{OC} \approx (AK_B\mathrm{T}/q\ )\mathrm{In}(J_{SC}/J_0) \quad (5)$$

Where R_S caused by electrode at the highest applied voltage. We calculate the A and J_0 from reverse *J-V* curves using formulas (3) and (4) [2, 3]. Formula (5) can calculate V_{OC} from J_0, J_{SC} and A that can check accuracy of J_0 and A. Figure S18a and S18b show the plots of -dV/dJ vs. $(J_{SC}\text{-}J)^{-1}$ and ln (J_{SC}-J) vs. V+$R_S$$J$, respectively. Figure S18c show the contributions of shunt resistance, diode, and series resistance can be identified into the dark current density-voltage characteristic. [4] Shockley equation in dark conditions

is given by:

$$J = J_0[\exp(q(V - JR_s)/AK_BT) - 1] + (V - JR_s)/R_{sh} \quad (6)$$

In shunt resistance domination region, since V is very small ($V \to 0$), and $R_{sh} \gg R_s$, formula (6) can be simplified as follows:

$$J \approx V/R_{sh} \quad (7)$$

The R_{sh} can be calculated from dark *J-V* curve, and the result shown in Figure S18d. The above calculated values are summarized in Table S2.

Table SI2: Photovoltaic parameters of the perovskite solar cells under reverse scan and extracted parameters.

ETL	**Light source**	**PCE (%)**	V_{OC} **(V)**	J_{SC} **(mA/cm²)**	**FF**	R_S (Ω·cm²)	R_{sh} (Ω·cm²)	A	J_0 (mA/cm²)
SnO_2-ETL	Solar simulator 100 mW/cm²	16.98	1.11	20.92	0.729	2.48	22281	2.58	2.15×10^{-6}
Pb-SnO_2/SnO_2		18.78	1.10	22.63	0.755	1.29	671140	1.45	1.38×10^{-11}

Analyze the relationship between J_{SC} and light intensity: When a weak bimolecular recombination occurs under short circuit, the J_{SC} obeys a power-law with respect to light intensity (P), J_{SC} *vs* P^{α}, α being close to 1[5, 6]. Whether under solar simulator or white-light LED, two samples' α values are very close 1.

Analyze the relationship between V_{OC} and light intensity: The V_{OC} usual dependence with the light intensity is expected to obey a linear relationship with the logarithm of the light intensity where the slope is equal to AK_BT/q [2, 7]. Regrettably, Figure 4d and 4f show some samples that the V_{OC} reduces rapidly and not obey a linear relationship with the logarithm of the light intensity under low-light conditions. Some articles had

appeared or mentioned the similar situation [5, 8, 9]. Therefore, the relationship between V_{OC} and J_{SC} is not enough to describe via A only. We need a more complete equivalent circuit of a solar cell, which has J_0, R_{sh} and R_S. The formula (1) can describe relationship between J and V, but that is transcendental in nature hence it is not possible to solve it for V in terms of J and vice versa. Therefore, explicit solution for J and V can be expressed using Lambert W function as follows:[1]

$$J = -\frac{V}{R_s + R_{sh}} + \frac{R_{sh}(J_0 + J_{ph})}{R_s + R_{sh}}$$

$$-\text{Lambert}W\left(\frac{R_S J_0 R_{sh} q \exp\left({}^{R_{sh}q(R_S J_{ph} + R_S J_0 + V)}/_{AK_BT(R_S + R_{sh})}\right)}{AK_BT(R_S + R_{sh})}\right) AK_BT/qR_s \qquad (8)$$

Substitute $J = 0$ in formula (8), explicit solution of V_{OC} is

$$V_{OC} = J_{ph}R_{sh} + J_0 R_{sh} - AK_B\text{T}/q\ \text{Lambert}W\left(\frac{J_0 R_{sh} q \exp\left({}^{-R_{sh}q(-J_{ph} - J_0)}/_{AK_BT}\right)}{AK_BT}\right) \qquad (9)$$

Lambert W function can also be called product log function, we solved it by Mathematica. Here, we obtained the simulated J-V curves from formula (8), and showed in Figure S19. We fixed the parameters ($J_0 = 1\times10^{-11}$ mA/cm^2, A = 1.5, $R_s = 1.2$ Ω·cm^2, T = 310K) that is reasonable value of perovskite solar cells, and obtained simulated J-V curves of different R_{sh} under different J_{ph}. J_{ph} usually obeys a power-law with respect to light intensity, so at the same device, different J_{ph} can indicate that under different light intensity. Under J_{ph} = 25 mA/cm^2 (around 1 sun condition), simulated J-V curves of different R_{sh} are very similar. But, under J_{ph} = 0.05 mA/cm^2 (low-light condition), the effect of R_{sh} on the J-V curve is obvious. For further study the relationship between V_{OC} and light intensity, simulated V_{OC}-J_{ph} relationship curves showed in Figure 6b and that according to formula (9). If R_s is much smaller than R_{sh}, J_{SC} can be approximately equal to J_{ph}. The simulated and measured V_{OC}-J_{SC} relationship

curves, are shown in Figure S20a, a similar method has been reported earlier in reference [9]. Here, a little deviation between calculated and measured values of V_{OC} should be mainly due to temperature and polarization. Under solar simulator, the increase in temperature is hard to avoid, which slightly reduces the V_{OC} of device[10]. Because the SnO2-PbO effectively reduced A, J_0, R_S and significantly increased R_{sh}, so SnO2-PbO devices have smaller V_{OC} losses than SnO_2 devices in low-light conduction.

Analyze the relationship between *FF* and light intensity: Besides V_{OC} and J_{SC}, *FF* are also very important parameters for the solar cells. We can obtain *FF* from formula (10):

$$FF = V_m J_m / V_{OC} J_{SC} = P_m / V_{OC} J_{SC} \quad (10)$$

V_m, J_m and P_m are optimum voltage, optimum current density, and maximum output power density respectively, corresponding to maximum power output condition. We can obtain V_m and J_m from the *J-V* curve. The simulated *FF*-J_{ph} relationship curves showed in Figure 6c. According to the simulative results, high R_{sh} is the key to keep high *FF* under low-light condition. The simulated and measured *FF*-J_{SC} relationship curves showed in Figure S20b. Simulated *FF* are bigger than measured that because of the simulated curves according to ideal single diode model. However, the experiment and simulation had similar changing rule.

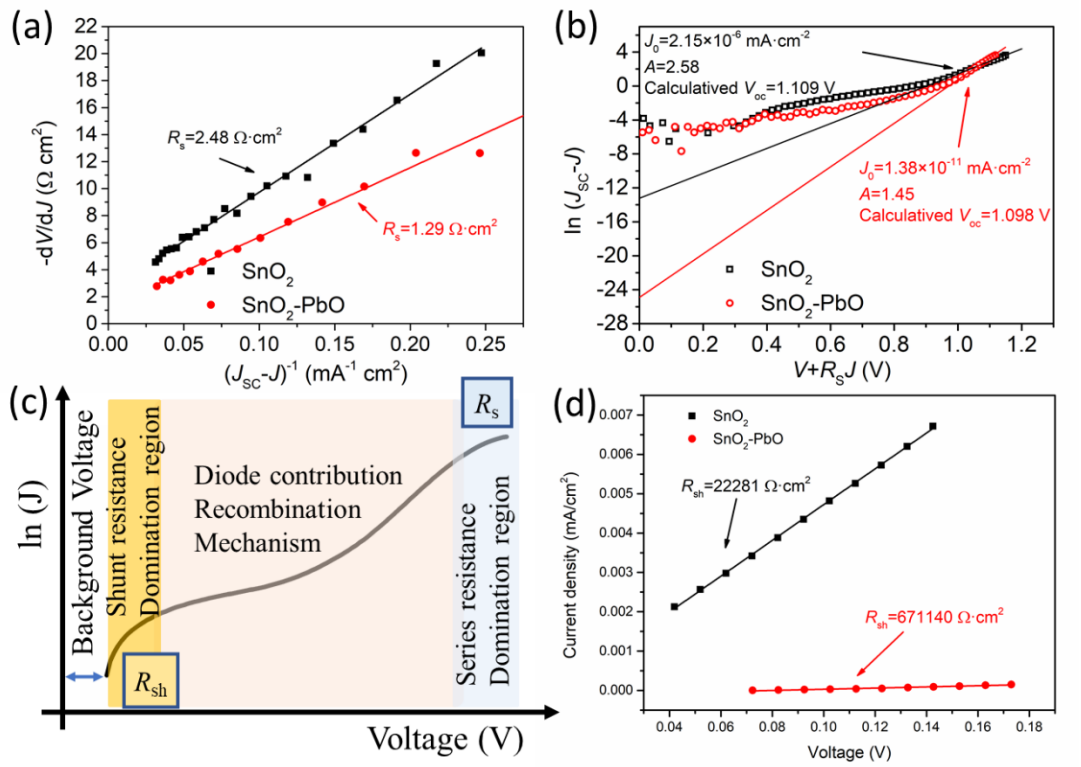

Figure S18. a) The linear curve of the relationship of $-dV/dJ$ *vs.* $(J_{SC}-J)^{-1}$. b) the plot of the relationship of ln $(J_{SC}-J)$ *vs.* $V+R_SJ$ of the perovskite solar cells based on different ETLs. c) the contributions of shunt resistance, diode, and series resistance can be identified into the dark current density-voltage characteristic. d) *J-V* curves measured in the dark and extraction of R_{sh}.

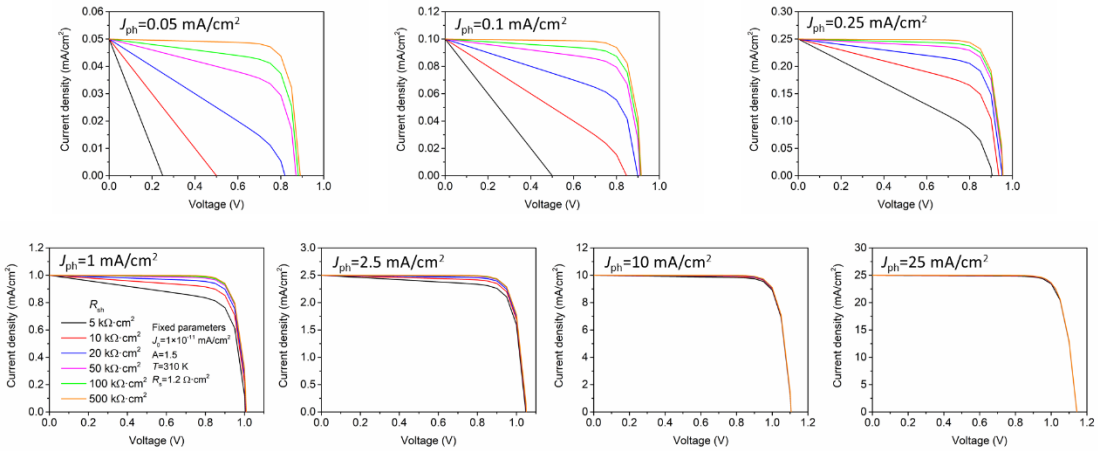

Figure S19. Simulated *J-V* curves for different R_{sh} under different J_{ph}.

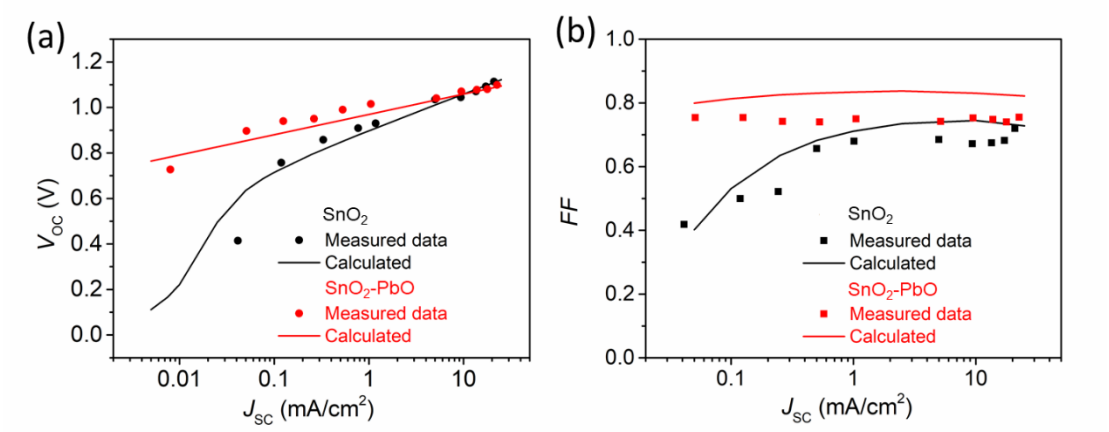

Figure S20. a) measured and calculated V_{OC}-J_{SC} curves and b) measured and calculated FF-J_{SC} curves of SnO_2 and SnO_2-PbO based PSCs.

References

[1] A. Jain, A. Kapoor, Sol Energ Mat Sol C 2004, 81, 269.

[2] J. J. Shi, X. Xu, D. M. Li, Q. B. Meng, Small 2015, 11, 2472.

[3] Z. N. Bi, Z. R. Liang, X. Q. Xu, Z. S. Chai, H. Jin, D. H. Xu, J. L. Li, M. H. Li, G. Xu, Sol Energ Mat Sol C 2017, 162, 13.

[4] A. Guerrero, B. Dorling, T. Ripolles-Sanchis, M. Aghamohammadi, E. Barrena, M. Campoy-Quiles, G. Garcia-Belmonte, Acs Nano 2013, 7, 4637; K. Tvingstedt, L. Gil-Escrig, C. Momblona, P. Rieder, D. Kiermasch, M. Sessolo, A. Baumann, H. J. Bolink, V. Dyakonov, Acs Energy Lett 2017, 2, 424; M. Barbato, M. Meneghini, A. Cester, G. Mura, E. Zanoni, G. Meneghesso, Ieee T Device Mat Re 2014, 14, 942.

[5] N. Guijarro, L. Yao, F. Le Formal, R. A. Wells, Y. P. Liu, B. P. Darwich, L. Navratilova, H. H. Cho, J. H. Yum, K. Sivula, Angew Chem Int Edit 2019.

[6] S. R. Cowan, A. Roy, A. J. Heeger, Phys Rev B 2010, 82.

[7] S. M. Sze, Cc/Eng Tech Appl Sci 1982, 28.

[8] S. W. Glunz, J. Dicker, M. Esterle, M. Hermle, J. Isenberg, F. J. Kamerewerd, J. Knobloch, D. Kray, A. Leimenstoll, F. Lutz, D. Osswald, R. Preu, S. Rein, E. Schaffer, C. Schetter, H. Schmidhuber, H. Schmidt, M. Steuder, C. Vorgrimler, G. Willeke, Conference Record of the Twenty-Ninth Ieee Photovoltaic Specialists Conference 2002 2002, 450; J. Dagar, S. Castro-Hermosa, G. Lucarelli, F. Cacialli, T. M. Brown, Nano Energy 2018, 49, 290; R. Steim, T. Ameri, P. Schilinsky, C. Waldauf, G. Dennler, M. Scharber, C. J. Brabec, Sol Energ Mat Sol C 2011, 95, 3256.

[9] N. Marinova, W. Tress, R. Humphry-Baker, M. I. Dar, V. Bojinov, S. M. Zakeeruddin, M. K. Nazeeruddin, M. Gratzel, Acs Nano 2015, 9, 4200.

[10] K. Nishioka, T. Sueto, M. Uchida, Y. Ota, J Electron Mater 2010, 39, 704; Y. H. Chen, S. Q. Tan, N. X. Li, B. L. Huang, X. X. Niu, L. Li, M. Z. Sun, Y. Zhang, X. Zhang, C. Zhu, N. Yang, H. C. Zai, Y. L. Wu, S. Ma, Y. Bai, Q. Chen, F. Xiao, K. W. Sun, H. P. Zhou, Joule 2020, 4, 1961.